

# Hadronic Trigger using electromagnetic calorimeter and particle identification at high- $p_T$ with STAR Detector

Hongyu Da<sup>a</sup>, Xiangli Cui<sup>a,b</sup>, Yichun Xu<sup>a</sup>, Lee Barnby<sup>e</sup>,  
Xin Dong<sup>c</sup>, J.C. Dunlop<sup>b</sup>, Lijuan Ruan<sup>b</sup>, Zebo Tang<sup>a</sup>,  
Anthony Timmins<sup>d</sup>, Gene Van Buren<sup>b</sup>, Zhangbu Xu<sup>b</sup>  
Xiaolian Wang<sup>a</sup>

<sup>a</sup>*Department of Modern Physics, University of Science and Technology of China,  
Hefei, Anhui, China, 230026*

<sup>b</sup>*Department of Physics, Brookhaven National Laboratory, Upton, NY 11973, USA*

<sup>c</sup>*Lawrence Berkeley National Laboratory, 1 Cyclotron Road, Berkeley, CA 94720,  
USA*

<sup>d</sup>*Physics Department, 617 Science & Research Building 1, Houston, TX 77204*

<sup>e</sup>*University of Birmingham, Birmingham, United Kingdom*

---

## Abstract

We derive a new method to improve the statistics of identified particles at high transverse momentum ( $p_T$ ) using online-triggered events by the Barrel Electro-Magnetic-Calorimeter (BEMC) detector. The BEMC is used to select hadronic interaction and energy deposit from showers created by charged hadrons ( $\pi^\pm, K^\pm$  and  $p(\bar{p})$ ) in the BEMC. With this trigger, the statistics of the high  $p_T$  particles are significantly enhanced by about a factor of 100 with selection efficiency up to 20%. In addition, resonant states ( $\rho^0, K^*$ ) and weak-decay V0 ( $K_S^0$  and  $\Lambda(\bar{\Lambda})$ ) can be constructed by selecting the BEMC-trigger hadron as one of its daughters. We also show that the trigger efficiency can be obtained reliably in simulation and data-driven approaches.

*Key words:* EMC, hadronic trigger, trigger efficiency

*PACS:* 29.40.Cs, 29.85.Fj

---



---

*Email address:* xuyichun@mail.ustc.edu.cn (Yichun Xu).

# 1 Introduction

One of the main physics goals of the Relativistic Heavy Ion Collider (RHIC) with the experiment of the Solenoidal Tracker at RHIC (STAR) in recent (and future) years is to study the properties of the Quark-Gluon-Plasma (QGP) created in the heavy ion collisions [1]. An important probe is to use the identified high- $p_T$  hadrons to study the color charge effect of parton energy loss in heavy ion collisions [2,3,4,5,6,7]. At RHIC, the luminosity is usually much higher than the detector and data acquisition capability. RHIC delivers  $p+p$  collision rates of several  $MHz$  while the STAR Time Projection Chamber (TPC) readout is around one  $kHz$ . Trigger detectors are used to implement an online selection of events of interest to the program. An example of such a detector is the electromagnetic calorimeter (EMC) used to select events with high energy deposit from an electromagnetic shower in the detector. This can enhance the event sample with high energy neutral pions or energetic jets with significant electromagnetic components ( $\pi^0$  or  $\gamma$ ). However, STAR has no hadronic calorimeter to select the final state charged hadrons although those hadrons do leave ionization tracks behind in the TPC or other tracking detectors. To date, charged hadron spectra in  $p+p$  and  $A+A$  collisions at RHIC have only been obtained using a minimum-bias trigger and their upper reach in  $p_T$  is severely limited by rapidly falling statistics at high- $p_T$  from such an all-inclusive trigger. For example, the charged pion spectra are so far only measured at RHIC to  $p_T \simeq 10 \text{ GeV}/c$  in  $p+p$  collisions, while the  $\pi^0$  spectra reach  $p_T \simeq 20 \text{ GeV}/c$ . On the other hand, the STAR EMC contains about one hadronic interaction length of material and can perform online trigger selection of events based on energy deposition in finely segmented towers. Charged hadrons do interact and produce showers with a significant amount of energy in the EMC at a lower efficiency.

In this paper, we present a study of hadronic trigger efficiency from the STAR Barrel EMC (BEMC). Different BEMC energy thresholds and BEMC patch sizes are used in this study. The inclusive charged hadron spectra are selected from the away-side opposite the struck calorimeter tower (or jet patch). PYTHIA simulations were performed to correct for the trigger effect. In addition to the enhancement of single hadron yields at high momentum, these triggers also allow us to construct resonances and weak-decay particles from their charged hadron daughters by requiring that one of the daughters produce a BEMC signal above the trigger threshold. The trigger effect on resonance and V0 reconstructions was corrected for using the experimental data. This approach avoids a demanding simulation of the details of the detector and trigger performances on the struck EMC tower. These allow us to not only extend the measurements of identified hadron spectra to much higher momentum, but also provide crucial consistency checks among different measurements in the same momentum range:  $\pi^0$  vs  $\pi^\pm$ ,  $K_s^0$  vs  $K^\pm$ . The current manuscript provides

the technical details of the triggers, analyses, correction and systematics while the scientific results have been discussed in Ref. [8].

## 2 Experimental Setup and Data Analysis

### 2.1 Detectors and Datasets

The data used for this study were collected with the STAR detector in the year 2005 [9,10]. Events were recorded requiring the minimum-bias trigger condition plus energy deposition in the BEMC detector for  $p + p$  collisions [11]. For this data, the total BEMC coverage is  $0 < \eta < 1$  and  $0 < \phi \leq 2\pi \text{ rad}$ . Each calorimeter tower covers  $\Delta\eta \times \Delta\phi = 0.05 \times 0.05 \text{ rad}$  in pseudo-rapidity ( $\eta$ ), and azimuthal angle ( $\phi$ ). The online energy deposition triggers utilize either a single BEMC tower (high tower trigger, HT) or a contiguous  $\Delta\eta \times \Delta\phi = 1 \times 1 \text{ rad}$  region (jet patch trigger, JP) of the BEMC [12]. A total of 5.6 million JP events with transverse energy  $E_T > 6.4 \text{ GeV}$  are used for  $\pi^\pm$ ,  $K^\pm$ , and  $p(\bar{p})$  analyses. To reduce trigger biases and to avoid the demandingly precise simulation of hadronic shower and the detector trigger response, only away-side particles (at azimuthal angles  $90^\circ - 270^\circ$  from the JP trigger) are used in the analyses of the inclusive single charged hadron spectra. The high-tower (HT) trigger condition requires the energy of a single calorimeter tower to be at least  $2.6 \text{ GeV}$  (HT1) or  $3.5 \text{ GeV}$  (HT2) [13,14]. In total, 5.1 million HT1 and 3.4 million HT2 events were collected from  $0.65 \text{ pb}^{-1}$  and  $2.83 \text{ pb}^{-1}$  integrated sampled luminosity of proton beams. These datasets are used for  $K_S^0 \rightarrow \pi^+ + \pi^-$ ,  $\bar{\Lambda} \rightarrow \bar{p} + \pi^+$  and  $\rho^0 \rightarrow \pi^+ + \pi^-$  reconstruction by requiring that one of the daughter pions or antiproton triggered the high tower.

The TPC covers  $0 < \phi \leq 2\pi$  and  $|\eta| \leq 1.3$  with up to 45 reconstructed hit points to serve as STAR's main tracking detector. It measures ionization energy loss ( $dE/dx$ ) and momentum (via curvature) of tracks in a  $0.5T$  solenoidal magnetic field, which together can provide particle identification, including along the relativistic rise at high momentum [15]. Topology of the daughter tracks from high- $p_T$   $K_S^0$ ,  $\Lambda(\bar{\Lambda})$ ,  $\rho^0$ ,  $K^*$ ,  $D^0$  and other resonances can be reconstructed through their hadronic decay into at least one high- $p_T$  charged hadron. In all of the analyses discussed here, the collision vertex is required to be within  $100 \text{ cm}$  of the TPC center. More details of hadron identification at high- $p_T$  [16,17,18] and topological V0 reconstruction of weak-decay particles [7] can be found in the references.

78 In addition to the required azimuthal angle between the track and the JP  
 79 trigger center to be  $|\Delta\phi| \geq \pi/2$  in the analyses of charged hadron spectra of  
 80  $\pi^\pm$ ,  $K^\pm$  and  $p(\bar{p})$ , the TPC tracks are selected based on:  $|\eta| < 0.5$ , track helix  
 81 projection to collision vertex in the Distance of Closest Approach (*gDCA*) to  
 82 be within 1.0 cm, number of TPC hits (*nHitsFit*) to be at least 25, number  
 83 of TPC hits to be at least 52% of the maximum possible hits and the TPC  
 84 hits involved in the  $dE/dx$  calculation (*ndEdxFit*) to be at least 15. In each  
 85  $p_T$  bin, the normalized  $dE/dx$ ,  $n\sigma_\pi$  [16,17,18,19] distributions of positively  
 86 and negatively charged particles are histogrammed. The detailed method of  
 87 calibration and extraction of raw counts of the individual identified hadrons  
 88 from the same data sample has been previously published [17].

89 The JP triggers enhance the statistics greatly, but also require additional  
 90 corrections with normalization and momentum-dependent efficiency. Figure 1  
 91 shows raw charged pion spectra in the BEMC-trigger events compared to the  
 92 published results (squares) in the minimum-bias events [3]. This shows that  
 93 charged pions in the BEMC-trigger data sample are enriched by an order  
 94 of magnitude at low  $p_T$  ( $\simeq 3 \text{ GeV}/c$ ) and by three orders of magnitude at  
 95 high  $p_T$  ( $\gtrsim 10 \text{ GeV}/c$ ). To correct for this trigger effect, PYTHIA events are  
 96 embedded into the STAR detector geometry in GEANT, which can simulate  
 97 the realistic response of the STAR detector. The Monte Carlo simulation is  
 98 based on PYTHIA version 6.205 [20] with CDF Tune A settings [21]. The same  
 99 simulation setup has been used in other jet related analyses [12]. In order to  
 100 fully cover the falling power-law spectrum in  $p_T$  of reconstructed particles  
 101 with sufficient statistics, the data samples were generated according to the  
 102 initial parton  $p_T$  intervals (in units of  $\text{GeV}/c$ ): (0,2), (2,3), (3,4), (4,5), (5,7),  
 103 (7,9), (9,11), (11,15), (15,25), (25,35) and ( $>35$ ). The spectra are weighted by  
 104 the cross-sections in each parton  $p_T$  range. Table 1 shows the absolute cross-  
 105 sections ( $\sigma_i$ ) for  $p + p$  collisions which generate the partons at each given  $p_T$   
 106 interval and the number of events ( $N_i$ ) going through the full simulation chain.  
 107 The obtained hadron spectra have to be weighted with the factor (proportional  
 108 to  $\sigma_i/N_i$ ) according to their originating partons.

109 The simulation includes detector response to the signal, electronic readout,  
 110 and detector and background noise when particles propagate through the de-  
 111 tector. The BEMC-trigger configuration and thresholds are then applied in  
 112 the same way as in the real events from experiment. The resulting charged  
 113 pion spectra from these simulations are shown on the left panel in Figure 1 for  
 114 the minimum-biased trigger and the BEMC-trigger events. The enhancement  
 115 of charged pions can be calculated by dividing the BEMC-trigger spectra by  
 116 the minimum-bias-trigger spectra from these PYTHIA simulations. The right  
 117 panel in Figure 1 shows the enhancement factor as a function of transverse

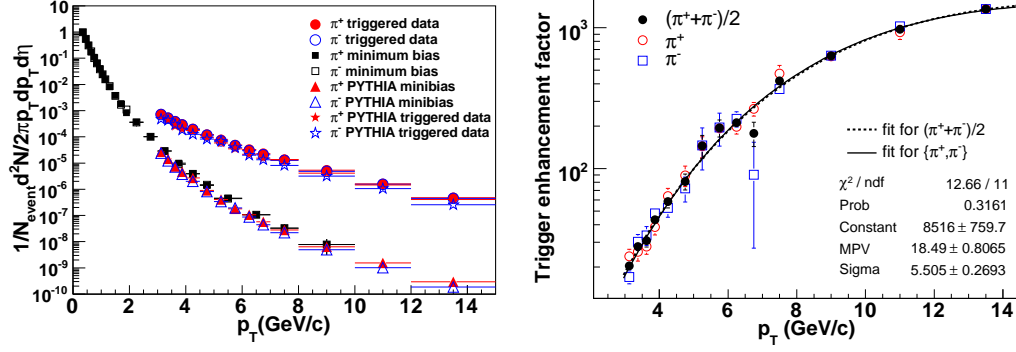


Fig. 1. The left panel shows pion spectra in minimum-bias and BEMC-trigger events from both measurements and the PYTHIA+GEANT simulation. Triggered enhancement from the simulations versus  $p_T$  distribution is shown on the right panel.

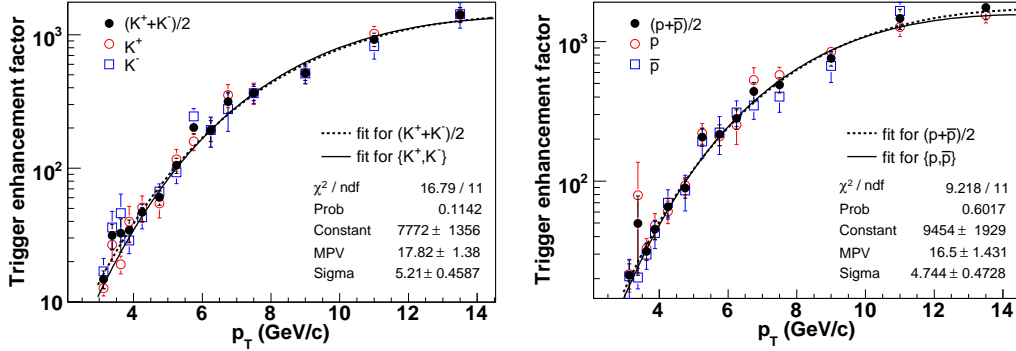


Fig. 2. Trigger enhancement factor distribution for kaon and proton are shown on the left panel and right panel respectively.

momentum. Similarly, the trigger enhancement factors for kaon and proton are calculated and presented in the left and right panels in Figure 2. These factors are then applied to the raw spectra to obtain the inclusive invariant differential cross-section of the charged hadrons in  $p + p$  collisions as presented in Ref. [8].

Since the correction for the JP trigger relies entirely on the PYTHIA event generator through the STAR detector simulation chain, concerns were raised whether the PYTHIA event generator simulates the jets and underlying event structure correctly and whether the detector simulation reproduces the JP trigger truthfully. To quantify this, several triggers with different jet-patch and high-tower energy thresholds have been used to study the systematic differences among the spectra after all the corrections have been applied, providing an estimate of the systematic uncertainty due to these effects. These are the largest contributions to the overall systematic uncertainties [8,6], especially at intermediate  $p_T$ .

Studies have shown that the underlying event structure [22] and the jet spec-

Table 1

Parton  $p_T$  interval, the corresponding absolute cross-section and the number of events generated in PYTHIA through the STAR simulation and reconstruction chain.

parton $p_T$ ( $GeV/c$ )	Cross-section ( $mb$ )	Number of events
(0,2)	18.2	339083
(2,3)	8.11	507996
(3,4)	1.30	400629
(4,5)	0.314	600980
(5,7)	1.36e-1	431000
(7,9)	2.31e-2	412000
(9,11)	5.51e-3	416000
(11,15)	2.22e-3	416000
(15,25)	3.89e-4	408000
(25,35)	1.02e-5	380000
( > 35)	5.30e-7	100000

tra [12] match well between data and PYTHIA. The results also show that the averaged  $\pi^\pm$  spectrum obtained from this method are consistent with the  $\pi^0$  spectra from both STAR [14] and PHENIX [23] to within 10%. The  $\pi^0$  spectra were obtained with a completely different trigger scheme: one of the photons from  $\pi^0$  decay has to be reconstructed from the BEMC high-tower, which triggers the event. Therefore, the  $\pi^0$  trigger is not affected by the event structure but depends on the simulation of the photon response and trigger efficiency. In the following sections, we describe a similar method to reconstruct resonances and V0 decays by using a BEMC high-tower as a hadronic trigger on one of the charged hadronic daughters. The trigger efficiency of the daughter hadrons is obtained directly from dividing the raw observed spectra of  $\pi^\pm$  and  $p(\bar{p})$  by their respective invariant spectra. Powerful consistency checks on trigger bias and  $K^\pm dE/dx$  uncertainty are possible by comparing the  $K^\pm$  spectra from jet away-side triggers and published minimum-bias-trigger results [7] with the invariant spectra of  $K_S^0 \rightarrow \pi^+ + \pi^-$  from our hadronic trigger.

### 2.3 Trigger enhancement and efficiency for hadrons

In this section, we provide the detailed procedure of obtaining the  $\pi^\pm$  and  $p(\bar{p})$  trigger efficiencies when either is associated with the high-tower that passes the online trigger threshold, where these are daughters from resonance

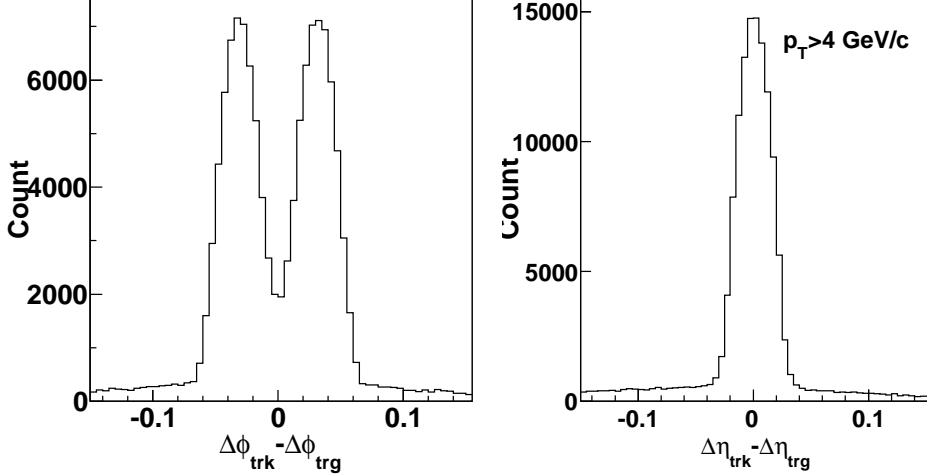


Fig. 3. The  $\Delta\phi$  and  $\Delta\eta$  between tracks and BEMC triggered towers. We note that the splitting into two peaks in  $\Delta\phi$  (i.e. in the bending plane) is due to the fact that the TPC track helices are projected to the BEMC surface while in reality the hadronic showers are on average deep within the BEMC.

153 ( $\rho^0 \rightarrow \pi^+ + \pi^-$ ) or V0 ( $K_S^0 \rightarrow \pi^+ + \pi^-$ ,  $\Lambda(\bar{\Lambda}) \rightarrow p(\bar{p}) + \pi^{-(+)}$ ) decays. In  
 154 offline analysis, a track reconstructed in the TPC is projected to the surface  
 155 of the BEMC and associated with a shower reconstructed from the BEMC  
 156 tower energies. The distances between the center of the triggered tower and  
 157 the track projections are shown in Figure 3. We require  $|\Delta\phi| < 0.075 \text{ rad}$  and  
 158  $|\Delta\eta| < 0.075$  for matched tracks. Projecting the backgrounds under the peaks,  
 159 we find that these cuts include  $\sim 3\%$  of accidental coincidences, most of which  
 160 will be further reduced by additional cuts.

161 Although hadronic interactions in an electromagnetic calorimeter develop show-  
 162 ers for which much of the energy escapes the detector, a significant fraction  
 163 of hadrons leave a sizable captured energy deposition. Figure 4 shows the  
 164 correlation between energy deposited in the triggered tower and momentum  
 165 of the matched track. The particles are selected between two cuts (shown in  
 166 the figure) on  $E \leq 2 \times p$ , to remove accidental coincidences with electromagnetic  
 167 showers, and  $E > 2 \text{ GeV}$ , to reject minimum ionizing particles and other low en-  
 168 ergy background coincidences. This provides a dataset with a wide momentum  
 169 range for further particle identification.

170 The normalized  $dE/dx$ ,  $n\sigma_\pi$  [16,17,18,19] distributions at  $3.25 < p_T < 3.50 \text{ GeV}/c$ ,  
 171 offset by +6 for positive particles and -6 for negative particles, are shown in  
 172 Figure 5. The peaks of triggered electrons and positrons are clearly separated  
 173 from charged hadrons. Statistics of charged pions and anti-protons are signif-  
 174 icantly enhanced in comparison to the distributions for minimum-bias-trigger  
 175 data [17]. The yield of triggered anti-protons is much larger than that of pro-  
 176 tons because they annihilate with the material in the BEMC and deposit an  
 177 additional  $\sim 2 \text{ GeV}$  extra energy.

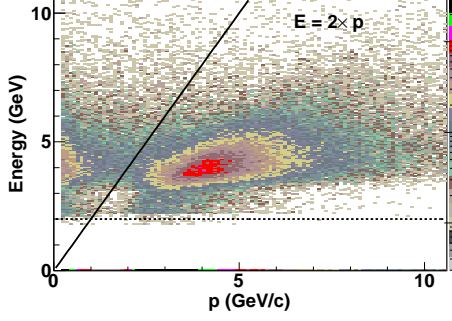


Fig. 4. Energy of triggered towers versus momentum of matched tracks. Only tracks with  $p_T > 3$  GeV/c were used in the analyses.

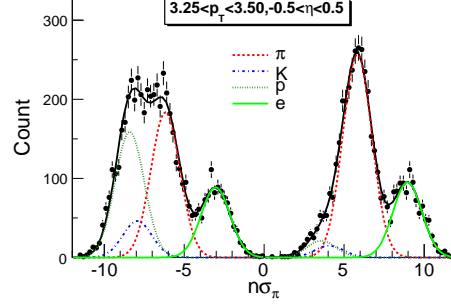


Fig. 5. Normalized  $dE/dx$  distributions at  $3.25 < p_T < 3.50$  GeV/c.

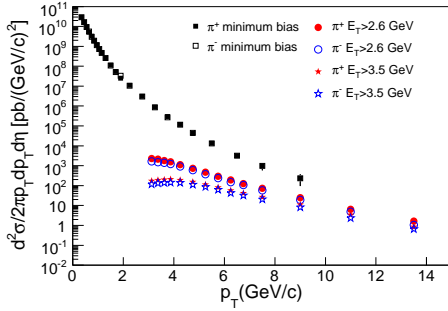


Fig. 6. pion  $p_T$  spectra from minimum-bias events and BEMC-trigger events.

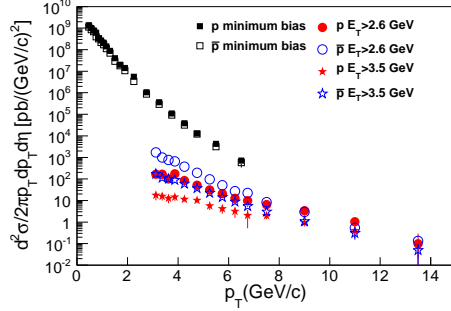


Fig. 7. proton  $p_T$  spectra from minimum-bias events and BEMC-trigger events.

Efficiencies can be derived by dividing the raw  $p_T$  spectra in the BEMC-trigger events by the inclusive invariant spectra obtained previously (shown in Figure 6 and Figure 7 respectively), and these efficiencies for pions and (anti-)protons are shown in Figure 8 and Figure 9. Although the efficiency is not as high as a pure electromagnetic shower, the trigger enhancement is quite high. Taking pion efficiency as an example, at  $p_T = 5$  GeV/c, the triggered pion efficiency in HT1 is  $\sim 2\%$ , and therefore the 5.1 million HT1 events (from  $0.65 \text{ pb}^{-1}$  sampled luminosity) are equivalent to luminosity  $(0.65 \text{ pb}^{-1}) \times \sigma_{pp}^{NSD}(30\text{mb}) \times [\text{trigger efficiency}](2\%) / [\text{tracking efficiency}](90\%) = \sim 450$  million minimum-bias-trigger (non-single diffractive [NSD]) events. This means a factor of  $\sim 100$  times more statistics for charged pions at this  $p_T$  in this data sample than in the previously published minimum-bias-trigger sample [2]. At higher  $p_T$ , the trigger efficiency and the minimum-bias event equivalents are much higher. The details can be found in Tables 2 and 3. Therefore, the BEMC-trigger data samples significantly enhance the available statistics of the particles at high  $p_T$ .



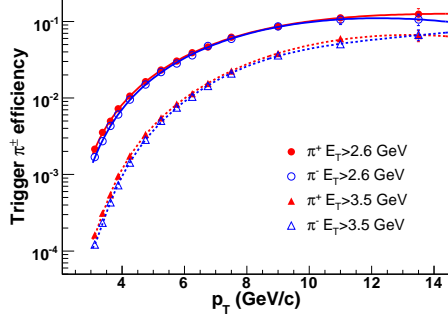


Fig. 8. Trigger efficiency and tracking efficiency of pion from BEMC-trigger events.

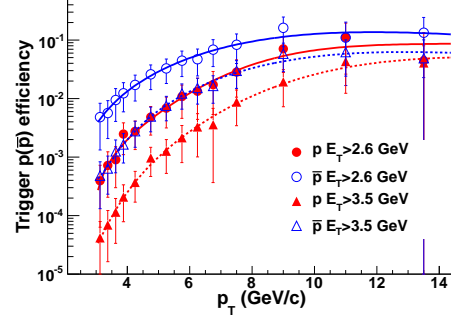


Fig. 9. Trigger efficiency and tracking efficiency of proton and pbar from BEMC-trigger events.

Table 2

The number of equivalent minimum-bias events ( $N_{eq}$ ) for charged pion at given  $p_T$  bin from 5.1 million HT1 and 3.4 million HT2 events respectively.

$p_T$	$N_{eq}(\pi^+) \text{ HT1}$	$N_{eq}(\pi^-) \text{ HT1}$	$N_{eq}(\pi^+) \text{ HT2}$	$N_{eq}(\pi^-) \text{ HT2}$
3.125	4.66e+07	3.61e+07	1.53e+07	1.16e+07
3.375	7.56e+07	6.11e+07	2.89e+07	2.15e+07
3.625	1.11e+08	9.28e+07	5.29e+07	4.10e+07
3.875	1.53e+08	1.32e+08	8.81e+07	7.08e+07
4.25	2.29e+08	2.03e+08	1.64e+08	1.37e+08
4.75	3.52e+08	3.21e+08	3.11e+08	2.68e+08
5.25	4.97e+08	4.64e+08	5.15e+08	4.54e+08
5.75	6.62e+08	6.30e+08	7.77e+08	6.97e+08
6.25	8.41e+08	8.11e+08	1.10e+09	9.98e+08
6.75	1.03e+09	1.00e+09	1.47e+09	1.35e+09
7.5	1.32e+09	1.30e+09	2.13e+09	1.97e+09
9	1.86e+09	1.83e+09	3.59e+09	3.38e+09
11	2.38e+09	2.26e+09	5.33e+09	5.02e+09
13.5	2.73e+09	2.32e+09	6.38e+09	5.92e+09

#### 194 2.4 Resonance and V0 reconstruction

195 The BEMC-trigger data sample not only increases the stable hadron yields to  
 196 tape, but also provides those high-statistic stable hadrons for the resonance  
 197 and V0 reconstructions. To reconstruct  $K_S^0$  or  $\Lambda(\bar{\Lambda})$  via their dominant weak  
 198 decay channels,  $K_S^0 \rightarrow \pi^+ + \pi^-$ ,  $\Lambda(\bar{\Lambda}) \rightarrow p(\bar{p}) + \pi^{-(+)}$ , we look for at least

Table 3

The number of equivalent minimum-bias events ( $N_{eq}$ ) for proton and anti-proton at given  $p_T$  bin from 5.1 million HT1 and 3.4 million HT2 events respectively.

$p_T$	$N_{eq}(p)$ HT1	$N_{eq}(\bar{p})$ HT1	$N_{eq}(p)$ HT2	$N_{eq}(\bar{p})$ HT2
3.125	7.88e+06	9.66e+07	3.75e+06	4.41e+07
3.375	1.59e+07	1.41e+08	6.79e+06	6.70e+07
3.625	2.53e+07	1.94e+08	1.17e+07	1.04e+08
3.875	3.66e+07	2.55e+08	1.90e+07	1.56e+08
4.25	5.77e+07	3.62e+08	3.53e+07	2.63e+08
4.75	9.61e+07	5.32e+08	7.01e+07	4.63e+08
5.25	1.50e+08	7.30e+08	1.25e+08	7.29e+08
5.75	2.24e+08	9.53e+08	2.06e+08	1.06e+09
6.25	3.19e+08	1.19e+09	3.18e+08	1.45e+09
6.75	4.38e+08	1.44e+09	4.69e+08	1.89e+09
7.5	6.56e+08	1.81e+09	7.77e+08	2.62e+09
9	1.16e+09	2.46e+09	1.68e+09	4.09e+09
11	1.66e+09	2.92e+09	3.20e+09	5.50e+09
13.5	1.86e+09	2.85e+09	4.53e+09	5.86e+09

one of the decay daughters to be the particle firing the BEMC trigger. The method is similar to the reconstruction of  $\pi^0 \rightarrow \gamma\gamma$  where the energy of at least one  $\gamma$  is above the BEMC-trigger threshold [14]. This procedure has also been used in the cross section measurement reported in Ref. [7,24].

The reconstructed event vertex is required to be along the beam axis and within 100 *cm* of the TPC center to ensure uniform tracking efficiency. A search is made in each event to find a (anti-)proton and pion tracks of the opposite curvature. The tracks are then paired to form a  $K_S^0$  or  $\Lambda(\bar{\Lambda})$  candidate and topological selections are applied to reduce backgrounds. Figures 10 and 11 show invariant mass distributions of the triggered  $K_S^0$  and  $\Lambda(\bar{\Lambda})$  at high  $p_T$  with only 5.1 million HT1 BEMC-trigger events, while 10 million minimum-bias events can only reach 5 *GeV/c* due to limited statistics [7].

To obtain the invariant spectra, we need to apply the correction factors due to the efficiencies of trigger, tracking and topological cuts. The correction is divided into two factors: kinematic efficiency and topological efficiency. The kinematic efficiency includes the effects of the BEMC response and trigger, the TPC tracking efficiency, and the acceptance due to kinematics. The topological efficiency includes the effects due to the topological requirements in

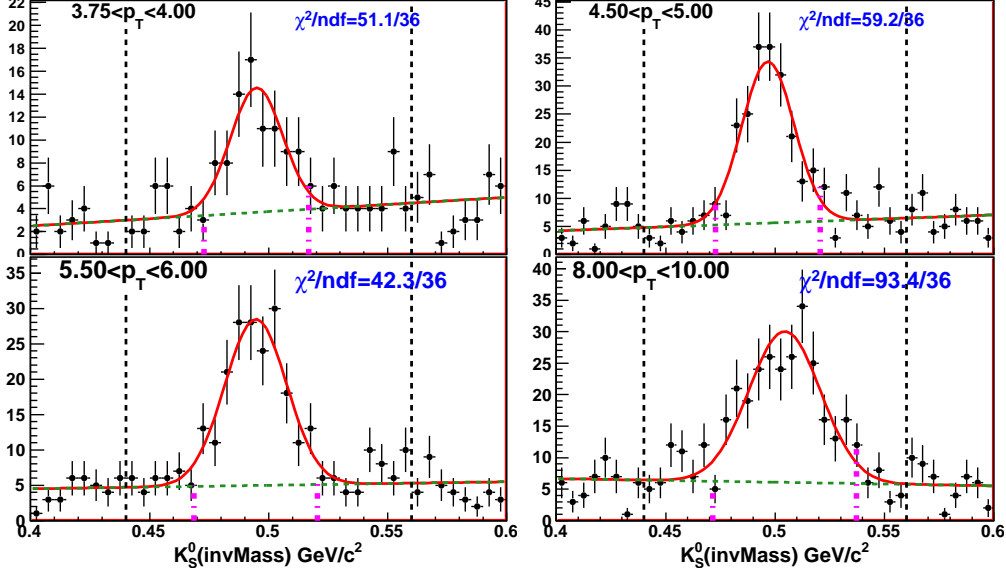


Fig. 10. Invariant mass of  $K_S^0$  at several high  $p_T$  bins.

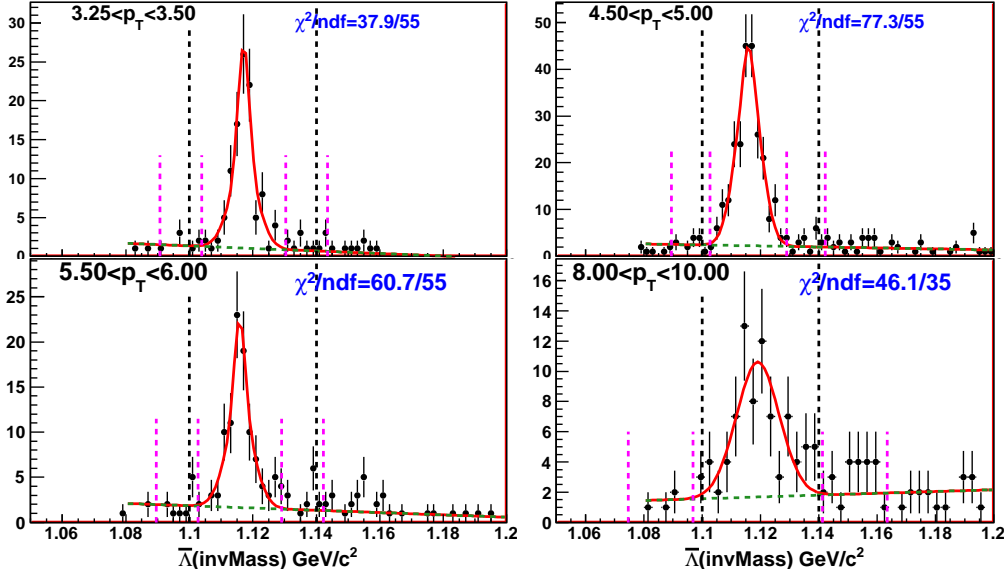


Fig. 11. Invariant mass of  $\bar{\Lambda}$  at several high  $p_T$  bins.

217 V0 reconstruction and is found to be  $p_T$  independent at 92% [7] for  $K_S^0$  (the  
 218 topological efficiencies of  $\Lambda(\bar{\Lambda})$  are still under study as of this writing). Fig-  
 219 ures 12, 13 and 14 are the kinematic efficiencies as a function of  $p_T$  for the  
 220 reconstruction of parent particles  $K_S^0$ ,  $\bar{\Lambda}$  and  $\rho^0$ , respectively.

221 Resonances ( $\rho^0 \rightarrow \pi^+ + \pi^-$ ,  $K^* \rightarrow K^\mp + \pi^\pm$  etc.) can be reconstructed in  
 222 a similar fashion. Since  $\rho^0$  decay strongly with a lifetime of about  $1\text{ fm}/c$ ,  
 223 reconstruction from its pion daughter pairs is made without the displaced de-  
 224 cay topological constraints used in V0 reconstruction. The invariant masses  
 225 of unlike-sign ( $\pi^+ + \pi^-$ ) and like-sign ( $\pi^\pm + \pi^\pm$ ) pion pairs are calculated and

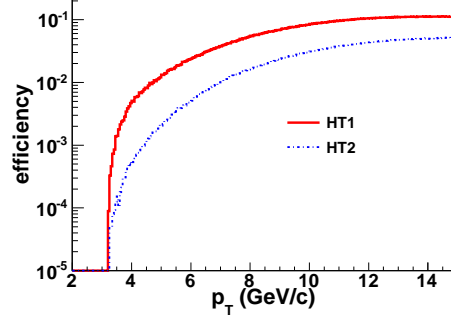
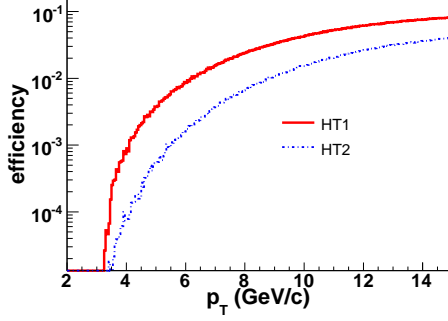


Fig. 12. Kinematic efficiency of  $K_S^0$  vs.  $p_T$ . Fig. 13. Kinematic efficiency of  $\bar{\Lambda}$  vs.  $p_T$ .

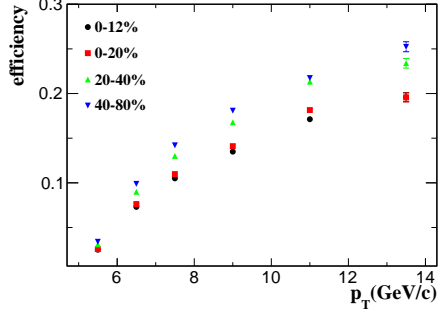


Fig. 14. Kinematic efficiency of  $\rho^0$  vs.  $p_T$ .

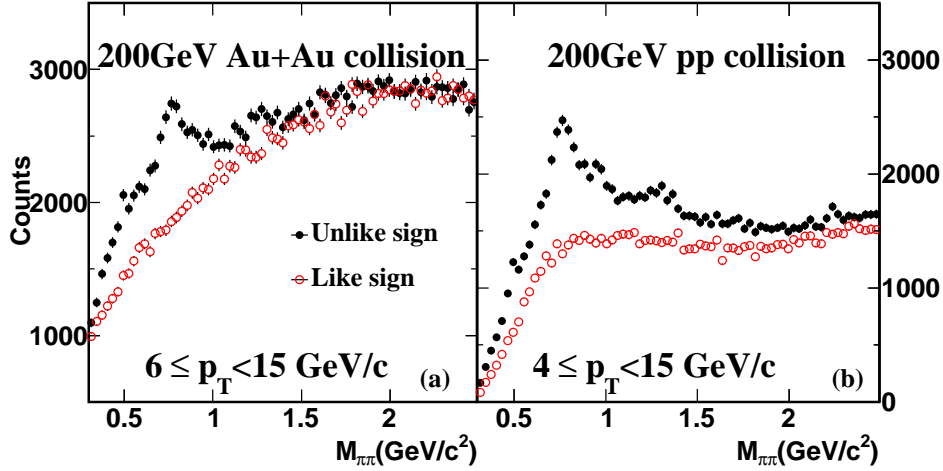


Fig. 15. Invariant mass distributions of the unlike-sign pairs  $\pi^+ + \pi^-$  and like-sign pairs  $\pi^\pm + \pi^\pm$  around the  $\rho^0$  mass. Panels (a) and (b) show the distributions from Au+Au and  $p + p$  collisions respectively.

226 shown in Figure 15. Panel (a) from this figure is for the invariant distribu-  
 227 tions in Au+Au collisions while panel (b) is for  $p + p$  collisions. The like-sign  
 228 pairs represent the random combinatoric background and the excess above  
 229 this background distribution in the unlike-sign is attributable to particle de-  
 230 cays ( $\rho^0$ ,  $\omega$ ,  $f_0$  and  $f_2$ ). Figure 16 shows the  $\pi^+ \pi^-$  invariant mass distribution  
 231 after like-sign background subtraction.

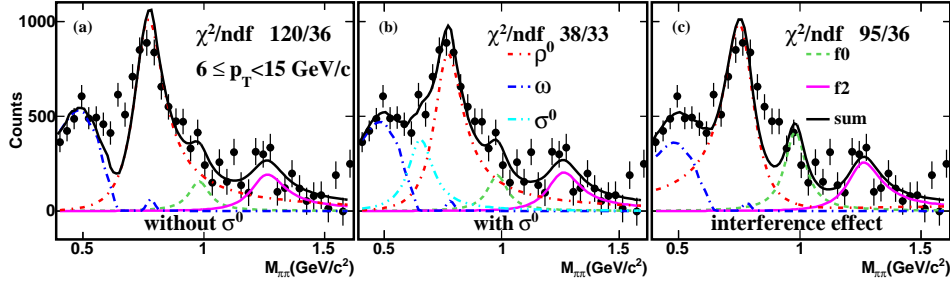


Fig. 16. Invariant mass distribution of  $\pi^+ + \pi^-$  around the  $\rho^0$  mass. The three panels show fits for (a) a four-species cocktail, (b) cocktail with additional  $\sigma^0$ , and (c) cocktail with an additional interference term.

For the line shape of  $\rho^0 \rightarrow \pi^+ + \pi^-$ , the procedure and formula from Ref. [25] were used with the  $\rho^0$  mass at  $775 \text{ MeV}/c^2$  and Breit-Wigner width  $155 \text{ MeV}/c^2$ . As with the low- $p_T$  case [25], a four-species cocktail describes the data quite well except that it under-describes data at invariant mass around  $600 \text{ MeV}/c^2$ . This is clearly visible in Figure 16(a). To investigate the possible missing components of the cocktail and how they impact the extracted  $\rho^0$  yields, we perform two additional studies by adding a  $\sigma^0$  to the cocktail and by adding an interference term between  $\rho^0 \rightarrow \pi^+ + \pi^-$  and direct  $\pi^+ + \pi^- \rightarrow \pi^+ + \pi^-$  scattering. Inclusion of the possible  $\sigma^0$  particle [26] (mass at  $\sim 600 \text{ MeV}/c^2$  and Breit-Wigner width scanning from 100 to  $500 \text{ MeV}/c^2$ ) results in 20% lower  $\rho^0$  yields and improves the  $\chi^2$  per degree of freedom ( $\chi^2/NDF$ ) from 120/36 to 38/33, a factor of nearly 3 improvement. This fit is shown in Figure 16(b) and is used to obtain the default  $\rho^0$  yields, where the  $\sigma^0/\rho^0$  ratio is about 25% independent of  $p_T$ . An additional systematic check is performed using the modified Soeding parametrization for a possible interference effect on the  $\rho^0$  line shape [27]. The parametrization and relative amplitudes of these two interference terms are from Ref. [27], which uses clear signals and well-defined processes in ultra-peripheral Au+Au collisions. Both the resulting  $\chi^2/NDF$  and the  $\rho^0$  yields fall between the other two fits. Figure 16(c) shows that the interference over-corrects the high-mass tail of the  $\rho^0$  spectral distribution and therefore under-predicts the data.

### 3 Summary

An electromagnetic calorimeter (the STAR BEMC) is leveraged to enhance the event sample containing charged hadrons at high transverse momentum, utilizing the STAR TPC for momentum reconstruction and species identification through  $dE/dx$ . The away-side hadrons opposite triggered jet patches (high collective energy in a group of BEMC towers) are used to provide spectra of charged hadrons at high  $p_T$ . Events triggered by high energy in a single BEMC tower are used to find hadronic shower candidates by matching these towers to

high  $p_T$  TPC tracks. These tracks are then paired with other charged hadrons to reconstruct  $K_S^0$ ,  $\Lambda(\bar{\Lambda})$  through their dominant decay channels:  $K_S^0 \rightarrow \pi^+ + \pi^-$  and  $\Lambda(\bar{\Lambda}) \rightarrow p(\bar{p}) + \pi^{-(+)}$ . With this method, spectra of the identified charged hadrons,  $K_S^0$ ,  $\Lambda(\bar{\Lambda})$  have been extended to higher  $p_T$  ( $\sim 12$  GeV/c) under the existing detector and RHIC luminosity capabilities [7]. This method is also used efficiently to extend the  $p_T$  reach for reconstructing strongly decaying particles, such as  $\rho^0$  and  $K^*$ .

## Acknowledgments

We thank the STAR Collaboration, the RHIC Operations Group and RCF at BNL, and the NERSC Center at LBNL for their support. This work was supported in part by the Offices of NP and HEP within the U.S. DOE Office of Science; Authors Yichun Xu and Zebo Tang are supported by National Natural Science Foundation of China under Grant No. 11005103 and No. 11005104, and Hongyu Da and Xiangli Cui are supported by the Knowledge Innovation Program of the Chinese Academy of Sciences, Grant No. kjc2-yw-a14, NSFC(10620120286, 10620120285).

## References

- [1] J. Adams *et al.* [STAR Collaboration], Nucl. Phys. A **757**, 102 (2005) [arXiv:nucl-ex/0501009].
- [2] L. Ruan [STAR Collaboration], J. Phys. G **34**, S199 (2007) [arXiv:nucl-ex/0701070]; J. Adams *et al.* [STAR Collaboration], Phys. Lett. B **616**, 8 (2005) [arXiv:nucl-ex/0309012]; B. I. Abelev *et al.* [STAR Collaboration], Phys. Lett. B **655**, 104 (2007) [arXiv:nucl-ex/0703040]; B.I. Abelev *et al.* [STAR Collaboration], Phys. Rev. Lett. **97**, 152301 (2006).
- [3] J. Adams *et al.* [STAR Collaboration], Phys. Lett. B **637**, 161 (2006) [arXiv:nucl-ex/0601033].
- [4] Yichun Xu (for STAR Collaboration) J. Phys. G: Nucl. Part. Phys. **37** (2010) 094059
- [5] Yichun Xu (for STAR Collaboration) Eur. Phys. J. C (2009) 62: 187
- [6] Yichun Xu (for STAR Collaboration) Nuclear Physics A 830 (2009) 701; Yichun Xu, PH.D. thesis, USTC 2009.
- [7] B. I. Abelev *et al.* [STAR Collaboration], Phys. Rev. C **75**, 064901 (2007).
- [8] STAR Collaboration (G. Agakishiev et al.), e-Print: arXiv:1110.0579.

- 294 [9] K. H. Ackermann *et al.* [STAR Collaboration], Nucl. Instrum. Meth. A 499, 624  
295 (2003).
- 296 [10] K. H. Ackermann *et al.* [STAR Collaboration], Nucl. Instrum. Meth. A **499**,  
297 624 (2003).
- 298 [11] M. Beddo *et al.* [STAR Collaboration], Nucl. Instrum. Meth. A **499** (2003) 725.
- 299 [12] B. I. Abelev *et al.*, Phys. Rev. D **79**, 112006 (2009); B. I. Abelev *et al.*, Phys.  
300 Rev. Lett. **100**, 232003 (2008); B. I. Abelev *et al.*, Phys. Rev. Lett. **97**, 252001  
301 (2006).
- 302 [13] F. S. Bieser *et al.*, Nucl. Instrum. Meth. A **499**, 766 (2003).
- 303 [14] B.I. Abelev et al., (STAR Collaboration) Phys. Rev. C **81** (2010) 64904
- 304 [15] M. Anderson *et al.*, Nucl. Instrum. Meth. A **499**, 679 (2003)  
305 [arXiv:nucl-ex/0205014].
- 306 [16] H. Bichsel, Nucl. Instrum. Meth. A **562** (2006) 154.
- 307 [17] Yichun Xu et al., Nuclear Instruments and Methods in Physics Research  
308 A614(2010)28.
- 309 [18] M. Shao *et al.*, Nucl. Instrum. Meth. A **558**, 419 (2006) [arXiv:nucl-ex/0505026].
- 310 [19] M. Aguilar-Benitez *et al.*, Z. Phys. C **50**, 405 (1991).
- 311 [20] T. Sjostrand *et al.*, Comput. Phys. Commun. **135**, 238 (2001)
- 312 [21] R. D. Field *et al.*, arXiv:hep-ph/0510198
- 313 [22] H. Caines [ STAR Collaboration ], Nucl. Phys. **A855**, 376-379 (2011).
- 314 [23] A. Adare *et al.* [PHENIX Collaboration], Phys. Rev. Lett. **101** (2008) 232301  
315 [arXiv:0801.4020 [nucl-ex]].
- 316 [24] Yan Lu, PH.D. Thesis, Central China Normal University Wuhan, 2005.
- 317 [25] J. Adams *et al.*, Phys. Rev. Lett. **92** (092301) 2004; B.I. Abelev *et al.*, Phys.  
318 Rev. C **78**, 044906 (2008).
- 319 [26] R. Garcia-Martin *et al.*, Phys. Rev. Lett. **107** (072001) 2011.
- 320 [27] B.I. Abelev *et al.*, Phys. Rev. C **77** (034910) 2008.